nature
COMMUNICATIONS

ARTICLE

1s-intraexcitonic dynamics in monolayer MoS$_2$ probed by ultrafast mid-infrared spectroscopy

Soonyoung Cha[1,*], Ji Ho Sung[2,3,*], Sangwan Sim[1], Jun Park[1], Hoseok Heo[2,3], Moon-Ho Jo[2,3] & Hyunyong Choi[1]

The 1s exciton—the ground state of a bound electron-hole pair—is central to understanding the photoresponse of monolayer transition metal dichalcogenides. Above the 1s exciton, recent visible and near-infrared investigations have revealed that the excited excitons are much richer, exhibiting a series of Rydberg-like states. A natural question is then how the internal excitonic transitions are interrelated on photoexcitation. Accessing these intraexcitonic transitions, however, demands a fundamentally different experimental tool capable of probing optical transitions from 1s 'bright' to np 'dark' states. Here we employ ultrafast mid-infrared spectroscopy to explore the 1s intraexcitonic transitions in monolayer MoS$_2$. We observed twofold $1s \rightarrow 3p$ intraexcitonic transitions within the A and B excitons and $1s \rightarrow 2p$ transition between the A and B excitons. Our results revealed that it takes about 0.7 ps for the 1s A exciton to reach quasi-equilibrium; a characteristic time that is associated with a rapid population transfer from the 1s B exciton, providing rich characteristics of many-body exciton dynamics in two-dimensional materials.

[1] School of Electrical and Electronic Engineering, Yonsei University, Seoul 120-749, Korea. [2] Center for Artificial Low Dimensional Electronic Systems, Institute for Basic Science (IBS), Pohang University of Science and Technology (POSTECH), Pohang 790-784, Korea. [3] Division of Advanced Materials Science, Pohang University of Science and Technology (POSTECH), Pohang 790-784, Korea. * These authors contributed equally to this work. Correspondence and requests for materials should be addressed to M-H.J. (email: mhjo@postech.ac.kr) or to H.C. (email: hychoi@yonsei.ac.kr).

Photogenerated electron-hole (e–h) pairs in solids create bound states, whose elementary quasiparticle state is called 1s exciton in a Wannier–Mott exciton model. Since the optoelectronic response is governed by the light-induced dynamic behaviour of this elementary ground state, knowledge of the 1s exciton response to the optical stimuli has been a crucial issue in many optoelectronic applications, such as phototransistors[1,2], photovoltaics[3], light-emitting diodes[4,5], van der Waals heterostructure-based optoelectronics[6–8] and valleytronic device applications[5,9–12]. In transition metal dichalcogenides (TMDCs), this is particularly the case as the two-dimensional (2D) materials approach a monolayer limit, where the reduced dielectric screening results in a strong Coulomb interaction[13–21], leading to an unusually large 1s exciton binding energy E_{bind}, typically a few hundreds of meV below the electronic bandgap of a few eV (refs 16,22–27).

Above the fundamental 1s exciton, theories predicted the presence of densely spaced exciton states in monolayer MoS_2 with 1s exciton E_{bind} of 0.4–0.54 eV (refs 18–21,28–31), whose (s-like) bright and (p-like) dark exciton characters were later confirmed by a series of seminal experiments via linear one-photon absorption[21,22], two-photon photoluminescence excitation (PLE)[22–24,32] and nonlinear wave-mixing spectroscopy[25,32], whereby E_{bind} was experimentally measured to be between 0.22 (ref. 26) and 0.44 eV (refs 23,26); the reported E_{bind}, however, shows somewhat discrepancy depending on the measurement methods and is varied from samples to samples[23,26,27]. These experimental techniques, although they are appropriate to clarify the optical state of the excitons, may address indirectly the dynamic transient information between the 1s 'bright' and the excited np 'dark' exciton (n is the principle quantum number); we denoted the exciton states in analogy to the hydrogen series[21]. By contrast, if one measures the 1s→np transitions, then the data should describe the internal excitonic transients, directly providing the transient optical nature of the fundamental 1s exciton dynamics. This, so called intraexcitonic spectroscopy[33], fundamentally differs from band-to-band and other time-resolved spectroscopies[8,34–36], and the technique can not only explain the transient response of the 1s exciton, but more importantly, may provide experimental manoeuvre in exploiting the photoinduced excitonic responses to the TMDC-based optoelectronic devices. For example, knowledge of the 1s and np exciton energies and their associated dynamics afford the first-order quantitative information on the exciton dissociation energy, where in an ideal case at least E_{bind}/e (e is the electron charge) of an external

or internal potential is required to dissociate the bound e–h pairs. In addition, because intraexcitonic spectroscopy can access the p-like dark excitons, one may design a scheme of coupling an infrared (IR) light to the 2D TMDC materials, via below-gap two-photon excitation, for the light-harnessing applications.

Here we explore the 1s intraexcitonic transient dynamics in monolayer MoS_2 by using time-resolved mid-IR spectroscopy. Inspired by a theoretical GW–Bethe–Salpeter result[19], where the fundamental 1s→2p transitions are predicted to be 0.32 and 0.3 eV for the A and B exciton in isolated, suspended monolayer MoS_2, we employed an ultrafast mid-IR spectroscopy (0.23–0.37 eV probe) in conjunction with an ultrafast white-light continuum spectroscopy (Fig. 1a). The mid-IR measurements show that there are two 1s→3p transitions for A and B exciton and 1s→2p between 1s A and 2p B exciton. The time-dependent IR absorption rapidly subdues over broad probe–photon energies, representing the transient absorption from the 1s to the quasi-continuum states after pump excitation.

Results

Time-resolved intraexcitonic and band-to-band dynamics. The samples used in our experiment were monolayer MoS_2, grown by chemical vapour deposition method, and were transferred to a CaF_2 substrate (see Supplementary Note 1 for the sample characterization). As schematically shown in Fig. 1a, the sample was non-resonantly excited by a 70 fs, 3.1 eV pump pulse, and the corresponding differential-transmission changes $\Delta T/T_0$ were measured in a vacuum cryostat (Methods). The 3.1 eV pump excites carriers into the quasi-continuum of the A and B excitons[37,38] or into the band-nesting C-band near the Γ point[39,40]. The former generates the unbound e–h plasma above the A and B excitons and the latter case experiences a rapid inter-valley scattering into K and K′ valley. Nevertheless, both cases generate carriers in much higher energy compared with the A or B exciton resonance. Figure 1b shows a direct comparison of two representative data measured by mid-IR probe (0.35 eV) and interband A-exciton probe (1.86 eV) with the same pump fluence $F = 24.4\ \mu J\ cm^{-2}$ (equivalent to e–h pair density of $7.4 \times 10^{12}\ cm^{-2}$ given 15% absorption)[8,41] measured at 77 K. The polarization of pump and probe beam are linear and orthogonal with respect to each other, such that we do not account for the recently discovered valley-exciton-locked selection rule[32]. The fact that two $\Delta T/T_0$ transients exhibit an opposite sign implies the kinetic origin of the photoresponses is indeed different. For the 1.86 eV dynamics, the increased
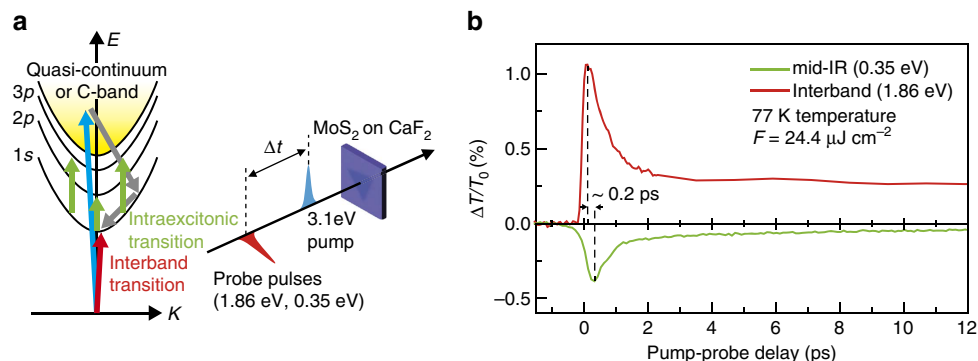

Figure 1 | Ultrafast intraexcitonic and band-to-band spectroscopy in monolayer MoS_2. (a) Schematic illustration of the ultrafast intraexcitonic (green) and conventional band-to-band (red) interband spectroscopy. The 3.1 eV optical pump (blue arrow) creates e–h pairs from ground to quasi-continuum states or C-band. The mid-IR pulse (green) measures the 1s→np transitions, while the white-light continuum pulse measures the ground-to-1s transition. (b) Transient dynamics of $\Delta T/T_0$ measured at two representative energies of 1.86 eV (red) and 0.35 eV (green). The positive sign of $\Delta T/T_0$ is observed for 1.86 eV probe, while 0.35 eV probe exhibits a negative sign. A clear temporal delay (~0.2 ps) between the two rising transients was observed. The experimentally determined temporal error bar for each time-zero (20 fs for 0.35 eV and 8 fs for 1.86 eV) is discussed in Supplementary Fig. 8.
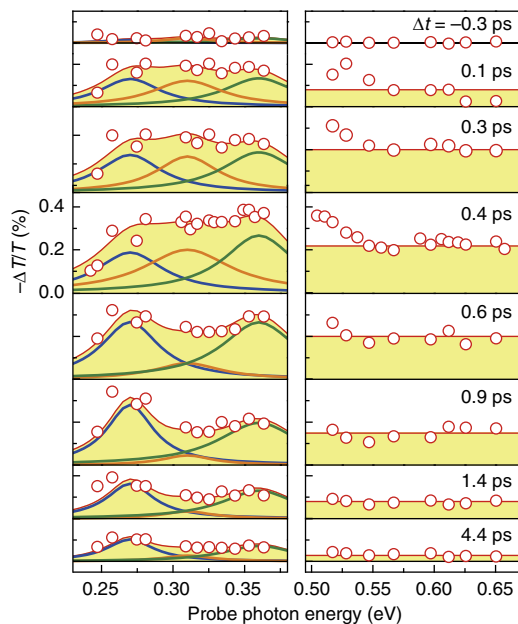
Figure 2 | Temporally and spectrally resolved transitions from 1s state.
Left panel is the mid-IR transient and right panel is the IR transient
dynamics. The transient spectra (red dots) are fitted by three Lorentzian
oscillators (blue, orange and green) for the mid-IR range and a step function
(red) for the IR range. The red solid in left panel is the sum of three
intraexcitonic oscillators. We note that it was not possible to fit all the mid-
IR spectra if only two oscillators were used.

probe transmission is typically attributed to the ground-state
bleaching[35,42,43], where the increased occupation probability of
electrons in conduction band and holes in the valance band leads
to the reduced probe absorption, that is, increased $\Delta T/T_0 > 0$. On
the other hand, given that the 0.35 eV probe is far below the
band-to-band A-exciton energy, one may attribute the decreased
$\Delta T/T_0 < 0$ (increased probe absorption) to the transition within
the bands, that is, intraband free-carrier absorption. However,
considering that the mid-IR peak signal is only 36.2% of the
1.86 eV one, we can exclude this possibility because the intraband
oscillator strength is much smaller than the interband one,
usually by an order of magnitude, as revealed by prior works on
the quasi-2D quantum wells[44] or recent 2D MoS$_2$ (ref. 45); as
discussed later in Figs 2–4, we provide compelling experimental
evidences to support our rationale (see also Supplementary
Note 2 (refs 46–48)). The increased probe absorption of the
mid-IR suggests that there exists an occupied state below the
electronic gap.

We find that there exists a clear time departure between the
two rising dynamics, where the onset of the 0.35 eV probe peak
appears ~0.2 ps later than the 1.86 eV probe (dashed line in
Fig. 1b). Immediately after the pump, the 1.86 eV probe rapidly
increases, while the 0.35 eV dynamics emerge rather slowly.
We observed that this rapid upsurge of the 1.86 eV is not a
local spectral behaviour, but being presented in a broad range of
high-energy probes (Supplementary Notes 3 and 4), evidencing
the quasi-instantaneous ground-state bleaching[35]. Understanding
this high-energy dynamics has been a subject to debate; different
investigations have proposed different kinetic origins of the 1s
exciton, such as exciton linewidth broadening[35], stimulated
emission[42], dynamic bandgap renormalization[49] and biexciton
formation[38]. As discussed, more details in Supplementary Note 4,
both earlier[50–52] and recent studies[35,42,53], have shown that the
3.1 eV photoexcitation into the quasi-continuum of unbound
states generates a significant amount of free-carriers. Because the

exciton formation occurs after exciton–free carrier scattering, the
initial decaying kinetics of mid-IR is slightly delayed compared
with the rising transient of the interband one, explaining the
observed time-delay between the two transients of Fig. 1b. Since
the mid-IR probe can resonantly measure the internal exciton
dynamics, the measured intraexcitonic transients are expected to
provide pure population dynamics of the ground 1s exciton[33,54].

Temporally and spectrally resolved intraexcitonic dynamics.
Figure 2 is the temporally and spectrally resolved mid-IR
dynamics. Here we probed not only the broad mid-IR transients
(0.23–0.37 eV), but also measured the IR dynamics
(0.47–0.67 eV). This scheme affords a simultaneous access to the
dynamic transitions from the 1s ground exciton to the higher
lying np excitons or quasi-continuum states. The measured
$-\Delta T/T_0$ spectra show peculiar energy-dependent behaviours. At
$\Delta t \leq 0.4$ ps, the $-\Delta T/T_0$ spectra are strongly reshaped, exhibiting
a relatively small increase of differential absorption (not absolute
absorption) near 0.27 eV compared with the increased absorption
around 0.3–0.5 eV. The increased absorption is more prominent
at $\Delta t > 0.4$ ps, where one can see that $-\Delta T/T_0$ is gradually larger
near 0.27 eV with increasing Δt, and the differential absorption at
0.3–0.5 eV is concurrently smaller with increasing Δt. Between
$0.4 < \Delta t \leq 0.9$ ps, $-\Delta T/T_0$ above 0.3 eV is rapidly vanished, while
the absorption resonance below 0.3 eV is accordingly increased.
After $\Delta t > 0.9$ ps, the absorption resonance below 0.3 eV keeps
reserved and it slowly subdues with featureless IR spectra
above 0.3 eV.

For a quantitative analysis of the observed transient spectra,
we use the following model consisted of multi-oscillator
components[55]:

$$\alpha(E) = \sum_n \frac{\hbar e^2 S_{1s-np}}{2mc\varepsilon_0\sqrt{\varepsilon}} \frac{\hbar\Gamma}{(E_n - E)^2 + (\hbar\Gamma)^2} + \Theta(E - E_{\text{bind}}). \quad (1)$$

The term of summation represents the intraexcitonic absorption
from 1s to either A or B excitonic np state and the second term
$\Theta(E - E_{\text{bind}})$ is a step-like transition[21] from 1s to the continuum
with E_{bind} of 0.44 eV. In the equation, ε (= 4.2) (refs 14,27) and ε_0
are the dielectric constant of monolayer MoS$_2$ and the vacuum
dielectric constant, respectively. There, the absorption amplitude
$S_{1s \to np}$, or the spectral weight of the intraexcitonic $1s \to np$
transition, is proportional to the product of the oscillator strength
$f_{1s \to np}$ and the ground exciton density n_{1s} (refs 39,40,55,56).
Because the 3.1 eV pump excitation creates e–h plasma in the
band nesting resonance, an accurate estimation of n_{1s} requires
both theoretical study of intervalley scatterings and the
corresponding ultrafast measurements, which is beyond the
scope of our ultrafast mid-IR intraexcitonic spectroscopy. In fact,
the spectral weight from $1s \to np$ is not only proportional to the
population, but also depends on the probability of finding an
empty final np state. As discussed about the transient spectra
dynamics above, the photoexcited unbound e–h pairs experience
rapid relaxation and start to form a ground-state exciton within
~0.4 ps. It is strictly true that the np exciton population is
negligible only at $\Delta t \geq 0.4$ ps. Similar studies on 1D and quasi-2D
quantum-well structures have shown that the contribution from
$np \to$ continuum is negligible[33,54,56–58]. We found that the
spectral fit matches well the measured data when we used up to
three mid-IR oscillators, with the following transition energy E_n
of $E_1 = 0.27$ eV, $E_2 = 0.31$ eV, and $E_3 = 0.36$ eV. On the basis that
the observed E_ns do not vary Δt, we fix E_n to fit the time-resolved
mid-IR spectra, but vary $S_{1s \to np}$ and the phenomenological
exciton broadening parameter Γ. For the IR transients, the
spectra are featureless representing the step-function-like 1s to
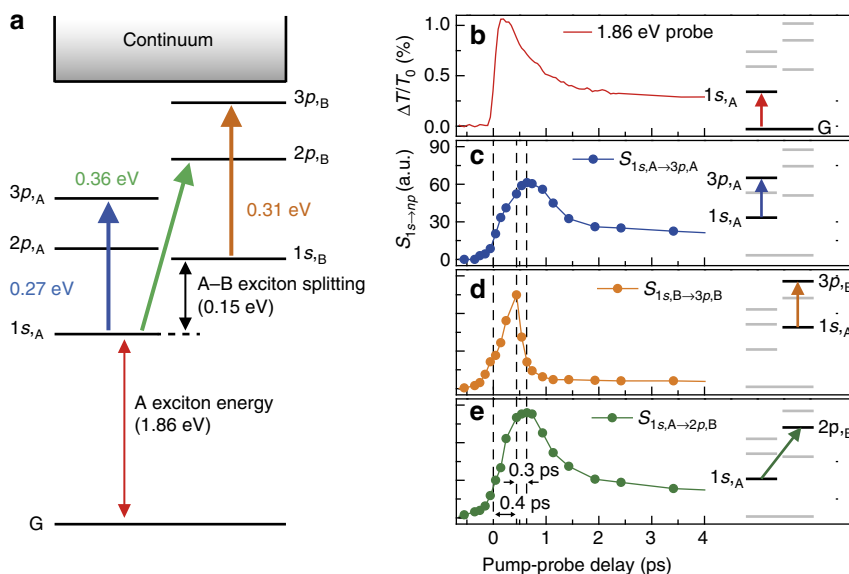the continuum transition[21]; this featureless IR spectrum is

Figure 3 | Schematic for 1s intraexcitonic transition and relevant spectral weight. (**a**) Energy diagram of the ground state (G), and the fundamental excitons ($1s_A$ and $1s_B$) and the higher excited np dark excitons in shown. Transition energies of three oscillators are indicated by blue (0.27 eV), orange (0.31 eV) and green (0.36 eV) arrows. The transient band-to-band dynamics (**b**) is directly compared with the intraexcitonic absorption dynamics (**c–e**). Transient dynamics of the intraexcitonic spectral weight parameter $S_{1s \to np}$ for each three oscillator are shown at each row: (**c**) $1s_A \to 3p_A$, (**d**) $1s_B \to 3p_B$ and (**e**) $1s_A \to 2p_B$, respectively. Dashed lines show the maximum $S_{1s \to np}$ peak for each intraexcitonic transition.
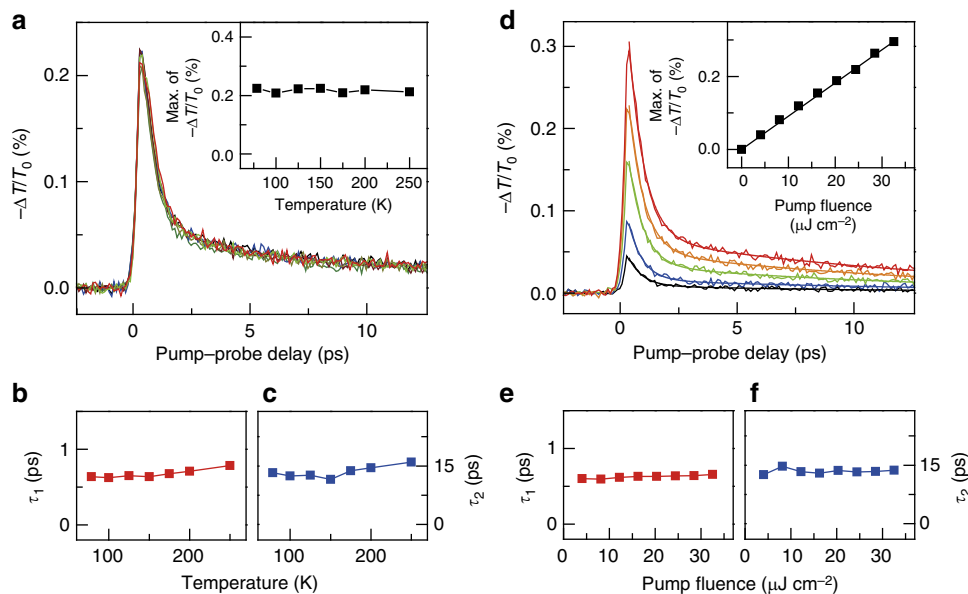

Figure 4 | Temperature- and fluence-dependent mid-IR dynamics. (**a**) Temperature-dependent $-\Delta T/T_0$ dynamics measured at 0.6 eV. Inset: the peak value of $-\Delta T/T_0$ is plotted as a function of the temperature. No temperature-dependent dynamics were observed, thereby the free-carrier absorption can be excluded in the analysis of Figs 1–3. We performed fitting using a biexponential function. The summarized results are shown in **b** for the fast τ_1 and in **c** for the slow decay component τ_2, where both components are temperature-independent. (**d**) Fluence-dependent $-\Delta T/T_0$ dynamics measured at 0.6 eV probe. Inset: the peak $-\Delta T/T_0$ shows a linear fluence dependence, such that no higher-order nonlinear exciton dynamics were observed. Fluence-dependent fast τ_1 (**e**) and slow decay component τ_2 (**f**). Solid line for each trace is the corresponding biexponential fit. Both τ_1 and τ_2 are independent of the pump fluence, implying that no absorption occurs from the defect states.

deviated from the step-like absorption at $\Delta t \leq 0.4$ ps, which might be due to the time-dependent thermalization process after the pump excitation.

Given that the magnitude of $S_{1s \to np}$ differs only by a factor of 2 for each E_n, these transitions cannot simply be assigned to the phenomena taking place within single exciton Rydberg series of the A (or B) exciton branch. This is because even when the nonhydrogenic excitonic nature of a monolayer TMDC is

considered, where a strongly (weakly) screened Coulomb potential is dominant when $n \leq 2$ ($n \geq 3$) (ref. 21), the spectral weight should be substantially decreased by nearly an order of magnitude with increasing n, which is too large to account for our measurement results. Of course, care should be taken to estimate the precise strength of intraexcitonic transition in a monolayer TMDC because the nonhydrogenic exciton is dominant when $n \leq 2$, thus the $1s \to np$ transition can deviate from the hydrogenic

excitonic nature for $n \geq 3$. This is because any intraexcitonic $1s \rightarrow np$ transition depends both on the wavefunction of the nth exciton as well as the $1s$ exciton state, and the latter certainly deviates from the 2D-hydrogen model. Recent PLE[23] revealed that the energy levels of the exciton Rydberg series are 1.88 eV ($1s$), 2.05 eV ($2s$) and 2.15 eV ($3s$) for A exciton and 2.03 eV ($1s$), 2.24 eV ($2s$) and 2.34 eV ($3s$) for B exciton. By considering 0.15 eV energy splitting between A and B excitons and the difference of reduced exciton masses of $0.25m_0$ (A exciton) and $0.28m_0$ (B exciton)[18], we estimated the intraexcitonic transition energies of 0.27 eV for $E_{1A \rightarrow 3A}$, 0.31 eV for $E_{1B \rightarrow 3B}$ and 0.36 eV for $E_{1A \rightarrow 2B}$, which are exactly matched our measured intraexcitonic transition energy E_n. Interestingly, these values are somewhat deviated from the GW–Bethe–Salpeter prediction[19], possibly due to the substrate dielectric screening effect. Nevertheless, our measurements agree well with the experimental PLE investigation due to similar dielectric constant of CaF_2 and fused silica[23] as a substrate. Although there is a small difference (~ 20 meV) for the A exciton energy between PLE (1.88 eV) and our photo-current spectra and ultrafast absorption measurement (1.86 eV, Supplementary Notes 1 and 3), the difference is very marginal[19,28,30,31] and the intraexcitonic spectroscopy can measure the energy difference between $1s$ and np, regardless of the A-exciton resonance. In accordance with PLE and our mid-IR measurements, we expect the fundamental $1s \rightarrow 2p$ would be 0.17 eV for the A exciton and 0.21 eV for the B exciton, and this is beyond our capability of tuning the mid-IR spectrum. Therefore, as schematically shown in Fig. 3a, we understand our intraexcitonic transition energy of E_1 as $1s_{,A} \rightarrow 3p_{,A}$ within A exciton, E_2 as $1s_{,B} \rightarrow 3p_{,B}$ within B exciton and E_3 as $1s_{,A} \rightarrow 2p_{,B}$ between A and B exciton. Indeed, our energy assignment well-corroborates a recent many-body Bethe–Salpeter prediction on the nonhydrogenic characters of excited excitons[19,20,28,30,31], underscoring a distinct capability of our intraexcitonic spectroscopy in measuring the relative energy difference between $1s$ and np. For the exciton broadening parameter Γ, since the effective mass of A and B exciton is different, Γ ($= 28.2$ meV) for $1s_{,A} \rightarrow 3p_{,A}$, Γ ($= 37.4$ meV) for $1s_{,B} \rightarrow 3p_{,B}$ and Γ ($= 30$ meV) for $1s_{,A} \rightarrow 2p_{,B}$ are slightly different due to the different exciton dispersion.

Dynamics of $1s \rightarrow np$ intraexcitonic spectral weights. For further analysis, we show the temporal dynamics of $S_{1s,A \rightarrow 3p,A}$ (Fig. 3c, blue), $S_{1s,B \rightarrow 3p,B}$ (Fig. 3d, orange) and $S_{1s,A \rightarrow 3p,A}$ (Fig. 3e, green). We identify three different kinetic regimes: immediately after the pump, the rising transients of all three spectral weights show similar behaviours, representing the hot-carrier relaxation from the quasi-continuum to the A and B exciton branch. This kinetics clearly differs from the dynamics of 1.86 eV probe (Fig. 3b), where the latter arises from the quasi-instantaneous bleaching dynamics. At $0.4 \leq \Delta t \leq 0.7$ ps, the dynamics of $S_{1s,B \rightarrow 3p,B}$ rapidly decrease, while the peak $S_{1s,A \rightarrow 3p,A}$ and $S_{1s,A \rightarrow 3p,B}$ emerge ~ 0.3 ps later. Because the $1s$ B exciton is 0.15 eV higher than that of A exciton (Fig. 3a), the $1s$ B exciton serves as a population supplier to the energetically lower $1s$ A exciton, thereby the two transients show a complementary dynamics. At longer $\Delta t > 0.7$ ps, because the $1s$ A excitons are thermalized and reaches a quasi-equilibrium condition, the dynamics of $S_{1s,A \rightarrow 3p,A}$ nearly follows that of $S_{1s,A \rightarrow 2p,B}$. This highlights that although $S_{1s,A \rightarrow 3p,A}$ and $S_{1s,A \rightarrow 3p,B}$ are spectrally separated apart, that is 0.27 and 0.36 eV, respectively, both transients are closely interrelated because these absorptions originate from the same $1s_{,A}$ ground state exciton.

Discussion

At an elevated temperature, the free-carrier absorption from $1s$, $2s$, $2p$, $3s$, $3p$ ... may contribute to the increased probe absorption

with $\Delta T/T_0 < 0$. This scenario typically shows a strong temperature dependence of the relaxation rate, in which the higher temperature the larger the electron–phonon scattering rate, resulting in the dynamics to be highly temperature dependent. Here given that the formation time scale of the $1s$ exciton is very fast within 0.4 ps (see Figs 2 and 3) and the Drude scattering rate cannot be extended to the mid-IR range (Supplementary Note 2), the contribution of $np \rightarrow$ continuum transition may be very insignificant to the temperature-dependent mid-IR intraexcitonic response. Figure 4a shows that our mid-IR transients, fitted by a biexponential function, exhibit nearly temperature independent of the relaxation components (Fig. 4b,c). This implies that the effect of free-carrier absorption is negligible. We additionally show in Fig. 4b that the recombination of excitons arises on sub-ps and tens of ps time scale. At $T = 77$ K, the mid-IR peak $|\Delta T/T_0|$ linearly increases with F up to 32.5 μJ cm^{-2} (equivalent to e–h pair density of 9.86×10^{12} cm^{-2}) (refs 8,41). The linear F-dependence reflects that there exists no high-order nonlinear excitonic interaction, ensuring that our mid-IR transients represent the first-order population dynamics. A recent below-gap-probe study[45] reported very similar relaxation times to our results. These time components were explained using defect-assisted exciton recombination. Given that we observed negligible F-dependent relaxation dynamics (Fig. 4e,f), we can infer that our mid-IR decay transients do not arise from the photoinduced absorption of filled e–h pair in the localized states, but arise from the exciton capture into the defects.

In summary, we report the experimental observation of the $1s$ intraexcitonic transition. Recently, Poellmann et al.[47] investigated a similar investigation of intraexcitonic transition in monolayer WSe_2, reporting the presence of strong absorption in a 2D TMDC, whose fundamental optical absorption originates from the $1s$ ground exciton. Our ultrafast mid-IR measurements reveal twofold $1s \rightarrow 3p$ transition energies to be 0.27 eV and 0.31 eV for A and B exciton, respectively. We additionally uncover an intraexcitonic relaxation channel of $1s \rightarrow 2p$ to be 0.36 eV between $1s$ A and $2p$ B exciton. The large exciton-binding energy due to the non-local dielectric screening ensures not only $1s \rightarrow 2p$ transition[47] to be observable, but also a higher-order transition of $1s \rightarrow 3p$ in a monolayer 2D TMDC at an elevated temperature, which cannot be accessible using conventional interband spectroscopy, or any in quasi-2D quantum-well structures. In addition, looking to the future, the availability of electric-gate tuning may enable to investigate the coherent many-body inter-excitonic correlations among exciton, biexciton[38,59] and trion[12,13,18,48] in a time-resolved controlled manner, which is non-trivial to study in other low-dimensional inorganic semiconductor structures.

Methods

Ultrafast optical pump–probe spectroscopy. Using 250 kHz, 50 fs Ti/sapphire laser system (Coherent RegA 9050), optical parametric amplifier (Coherent OPA 9850) yields signal (0.77–1.12 eV) and idler (0.47 eV–0.67 eV) pulses that are used to generate mid-IR pulse (0.23–0.37 eV) via difference frequency generator (Coherent DFG). The idler and DFG output serve as the probe pulse in the IR and mid-IR range, respectively. The chirp of mid-IR pulse is discussed in Supplementary Note 5. High-energy interband response was measured by using a white-light continuum (1.76–2.03 eV) generated by focusing 1.55 eV pulses into a 1 mm sapphire disk. For the group-delay dispersion (GDD) of the white-light continuum pulse, we compensated using a pair of prism, and further checked the GDD-induced delay via cross-correlation of the white-light pulse and 1.55 eV pulse, whose details are explained in the Supplementary Note 3. The 3.1 eV pump pulse was created by second harmonic generation of 1.55 eV pulse in a 1-mm-thick beta barium borate (BBO) crystal. Due to the combination of OPA and DFG, where both signal and idler from OPA were used to generate the mid-IR DFG output, the only available seed pulse for 3.1 eV pump pulse was 1.55 eV in our system, so that the mid-IR measurement with resonant pump excitation at either A or B $1s$ exciton was not possible in our current system. For the each mid-IR or IR measurement, pump pulse and probe pulse are simultaneously focused on the sample in the

cryostat equipped with two CaF_2 windows, and pump–probe delay is controlled by a mechanical delay stage (Newport M-IMS300LM). The spot size of our pump and probe beams were 100 µm, and 50 µm, respectively, which were simultaneously focused using $f = 50$ mm lens before the temperature-controlled vacuum cryostat. In our optical geometry, the 3.1 eV pump passes through a mechanical delay stage, so called 'pump delay'. Because the pump delay is recorded in a computer as an absolute length, we performed cross-correlation measurement to estimate the probe delay using BBO (visible upconversion) and KTA (mid-IR upconversion) crystals. More detailed information for determining the pump–probe 'time-zero' is explained in Supplementary Note 6. Differential transmission signal ($\Delta T/T_0$) was recorded in a lock-in amplifier (Stanford Research Systems SR850) with 10 kHz chopping frequency (Scitec 300CD). The schematics of mid-IR and IR setup are illustrated in the Supplementary Fig. 9.

References

1. Lopez-Sanchez, O., Lembke, D., Kayci, M., Radenovic, A. & Kis, A. Ultrasensitive photodetectors based on monolayer MoS_2. Nat. Nano 8, 497–501 (2013).
2. Wang, Q. H., Kalantar-Zadeh, K., Kis, A., Coleman, J. N. & Strano, M. S. Electronics and optoelectronics of two-dimensional transition metal dichalcogenides. Nat. Nano 7, 699–712 (2012).
3. Furchi, M. M., Pospischil, A., Libisch, F., Burgdorfer, J. & Mueller, T. Photovoltaic effect in an electrically tunable van der Waals heterojunction. Nano Lett. 14, 4785–4791 (2014).
4. Cheng, R. et al. Electroluminescence and Photocurrent generation from atomically sharp WSe_2/MoS_2 heterojunction p–n diodes. Nano Lett. 14, 5590–5597 (2014).
5. Zhang, Y., Oka, T., Suzuki, R., Ye, J. & Iwasa, Y. Electrically switchable chiral light-emitting transistor. Science 344, 725–728 (2014).
6. Britnell, L. et al. Strong light-matter interactions in heterostructures of atomically thin films. Science 340, 1311–1314 (2013).
7. Lee, C.-H. et al. Atomically thin pn junctions with van der Waals heterointerfaces. Nat. Nano 9, 676–681 (2014).
8. He, J. et al. Electron transfer and coupling in graphene–tungsten disulfide van der Waals heterostructures. Nat. Commun. 5, 5622 (2014).
9. Gong, Z. et al. Magnetoelectric effects and valley-controlled spin quantum gates in transition metal dichalcogenide bilayers. Nat. Commun. 4, 2053 (2013).
10. Xu, X., Yao, W., Xiao, D. & Heinz, T. F. Spin and pseudospins in layered transition metal dichalcogenides. Nat. Phys. 10, 343–350 (2014).
11. Mak, K. F., McGill, K. L., Park, J. & McEuen, P. L. The valley Hall effect in MoS_2 transistors. Science 344, 1489–1492 (2014).
12. Jones, A. M. et al. Optical generation of excitonic valley coherence in monolayer WSe_2. Nat. Nano 8, 634–638 (2013).
13. Mak, K. F., Lee, C., Hone, J., Shan, J. & Heinz, T. F. Atomically thin MoS_2: a new direct-gap semiconductor. Phys. Rev. Lett. 105, 136805 (2010).
14. Cheiwchanchamnangij, T. & Lambrecht, W. R. Quasiparticle band structure calculation of monolayer, bilayer, and bulk MoS_2. Phys. Rev. B 85, 205302 (2012).
15. Mak, K. F. et al. Tightly bound trions in monolayer MoS_2. Nat. Mater. 12, 207–211 (2013).
16. Ugeda, M. M. et al. Giant bandgap renormalization and excitonic effects in a monolayer transition metal dichalcogenide semiconductor. Nat. Mater. 13, 1091–1095 (2014).
17. Zhang, Y. et al. Direct observation of the transition from indirect to direct bandgap in atomically thin epitaxial $MoSe_2$. Nat. Nano 9, 111–115 (2014).
18. Berkelbach, T. C., Hybertsen, M. S. & Reichman, D. R. Theory of neutral and charged excitons in monolayer transition metal dichalcogenides. Phys. Rev. B 88, 045318 (2013).
19. Qiu, D. Y., Felipe, H. & Louie, S. G. Optical spectrum of MoS_2: many-body effects and diversity of exciton states. Phys. Rev. Lett. 111, 216805 (2013).
20. Berghäuser, G. & Malic, E. Analytical approach to excitonic properties of MoS_2. Phys. Rev. B 89, 125309 (2014).
21. Chernikov, A. et al. Exciton binding energy and nonhydrogenic rydberg series in monolayer WS_2. Phys. Rev. Lett. 113, 076802 (2014).
22. He, K. et al. Tightly bound excitons in monolayer WSe_2. Phys. Rev. Lett. 113, 026803 (2014).
23. Hill, H. M. et al. Observation of excitonic Rydberg states in monolayer MoS_2 and WS_2 by photoluminescence excitation spectroscopy. Nano Lett. 15, 2992–2997 (2015).
24. Ye, Z. et al. Probing excitonic dark states in single-layer tungsten disulphide. Nature 513, 214–218 (2014).
25. Wang, G. et al. Giant enhancement of the optical second-harmonic emission of WSe_2 monolayers by laser excitation at exciton resonances. Phys. Rev. Lett. 114, 097403 (2015).
26. Zhang, C., Johnson, A., Hsu, C.-L., Li, L.-J. & Shih, C.-K. Direct imaging of band profile in single layer MoS_2 on graphite: quasiparticle energy gap, metallic edge states, and edge band bending. Nano Lett. 14, 2443–2447 (2014).
27. Klots, A. R. et al. Probing excitonic states in suspended two-dimensional semiconductors by photocurrent spectroscopy. Sci. Rep. 4, 6608 (2014).
28. Berkelbach, T. C., Hybertsen, M. S. & Reichman, D. R. Bright and dark singlet excitons via linear and two-photon spectroscopy in monolayer transition metal dichalcogenides, Preprint at http://arxiv.org/abs/1505.07127 (2015).
29. Stroucken, T. & Koch, S. W. Evidence for optically bright p-excitons in transition-metal dichalchogenides, Preprint at http://arxiv.org/abs/1404.4238v2 (2014).
30. Wu, F., Qu, F. & MacDonald, A. H. Exciton band structure of monolayer MoS_2. Phys. Rev. B 91, 075310 (2015).
31. Chaves, A., Low, T., Avouris, P., Çakır, D. & Peeters, F. Anisotropic exciton Stark shift in black phosphorus. Phys. Rev. B 91, 155311 (2015).
32. Xiao, J. et al. Optical selection rule based on valley-exciton locking for 2D valleytronics, Preprint at http://arxiv.org/abs/1504.04947 (2014).
33. Kaindl, R. A., Carnahan, M. A., Hägele, D., Lövenich, R. & Chemla, D. S. Ultrafast terahertz probes of transient conducting and insulating phases in an electron–hole gas. Nature 423, 734–738 (2003).
34. Shi, H. et al. Exciton dynamics in suspended monolayer and few-layer MoS_2 2D crystals. ACS Nano 7, 1072–1080 (2013).
35. Sim, S. et al. Exciton dynamics in atomically thin MoS_2: interexcitonic interaction and broadening kinetics. Phys. Rev. B 88, 075434 (2013).
36. Hong, X. et al. Ultrafast charge transfer in atomically thin MoS_2/WS_2 heterostructures. Nat. Nano 9, 682–686 (2014).
37. Cabo, A. G. et al. Observation of ultrafast free carrier dynamics in single layer MoS_2. Nano Lett. 15, 5883–5887 (2015).
38. Sie, E. J., Frenzel, A. J., Lee, Y.-H., Kong, J. & Gedik, N. Intervalley biexcitons and many-body effects in monolayer MoS_2. Phys. Rev. B 92, 125417 (2015).
39. Carvalho, A., Ribeiro, R. & Neto, A. C. Band nesting and the optical response of two-dimensional semiconducting transition metal dichalcogenides. Phys. Rev. B 88, 115205 (2013).
40. Kozawa, D. et al. Photocarrier relaxation pathway in two-dimensional semiconducting transition metal dichalcogenides. Nat. Commun. 5, 4543 (2014).
41. Li, Y. et al. Measurement of the optical dielectric function of monolayer transition-metal dichalcogenides: MoS_2, $MoSe_2$, WS_2, and WSe_2. Phys. Rev. B 90, 205422 (2014).
42. Mai, C. et al. Many-body effects in valleytronics: direct measurement of valley lifetimes in single-layer MoS_2. Nano Lett. 14, 202–206 (2013).
43. Mai, C. et al. Exciton valley relaxation in a single layer of WS_2 measured by ultrafast spectroscopy. Phys. Rev. B 90, 041414 (2014).
44. Klimov, V., Schwarz, C. J., McBranch, D., Leatherdale, C. & Bawendi, M. Ultrafast dynamics of inter-and intraband transitions in semiconductor nanocrystals: Implications for quantum-dot lasers. Phys. Rev. B 60, R2177 (1999).
45. Wang, H., Zhang, C. & Rana, F. Ultrafast dynamics of defect-assisted electron–hole recombination in monolayer MoS_2. Nano Lett. 15, 339–345 (2015).
46. Shen, C.-C. et al. Charge dynamics and electronic structures of monolayer MoS_2 films grown by chemical vapor deposition. Appl. Phys. Exp. 6, 125801 (2013).
47. Poellmann, C. et al. Resonant internal quantum transitions and femtosecond radiative decay of excitons in monolayer WSe_2. Nat. Mater. 14, 889–893 (2015).
48. Lui, C. H. et al. Trion-induced negative photoconductivity in monolayer MoS_2. Phys. Rev. Lett. 113, 166801 (2014).
49. Wang, Q. et al. Valley carrier dynamics in monolayer molybdenum disulfide from helicity-resolved ultrafast pump–probe spectroscopy. ACS Nano 7, 11087–11093 (2013).
50. Wake, D. R., Yoon, H. W., Wolfe, J. P. & Morkoç, H. Response of excitonic absorption spectra to photoexcited carriers in GaAs quantum wells. Phys. Rev. B 46, 13452–13460 (1992).
51. Knox, W. H. et al. Femtosecond excitation of nonthermal carrier populations in GaAs quantum wells. Phys. Rev. Lett. 56, 1191–1193 (1986).
52. Knox, W. H., Chemla, D. S., Livescu, G., Cunningham, J. E. & Henry, J. E. Femtosecond carrier thermalization in dense Fermi seas. Phys. Rev. Lett. 61, 1290–1293 (1988).
53. Chernikov, A., Ruppert, C., Hill, H. M., Rigosi, A. F. & Heinz, T. F. Population inversion and giant bandgap renormalization in atomically thin WS_2 layers. Nat. Photon. 9, 466–470 (2015).
54. Wang, J., Graham, M. W., Ma, Y., Fleming, G. R. & Kaindl, R. A. Ultrafast spectroscopy of midinfrared internal exciton transitions in separated single-walled carbon nanotubes. Phys. Rev, Lett. 104, 177401 (2010).
55. Jörger, M., Fleck, T., Klingshirn, C. & Von Baltz, R. Midinfrared properties of cuprous oxide: High-order lattice vibrations and intraexcitonic transitions of the 1s paraexciton. Phys. Rev. B 71, 235210 (2005).
56. Huber, R., Kaindl, R. A., Schmid, B. A. & Chemla, D. S. Broadband terahertz study of excitonic resonances in the high-density regime in GaAs. $Al_xGa_{1-x}As$ quantum wells. Phys. Rev. B 72, 161314 (2005).

57. Suzuki, T. & Shimano, R. Time-resolved formation of excitons and electron-hole droplets in Si studied using terahertz spectroscopy. *Phys. Rev. Lett.* **103,** 057401 (2009).
58. Kaindl, R. A., Hägele, D., Carnahan, M. A. & Chemla, D. S. Transient terahertz spectroscopy of excitons and unbound carriers in quasi-two-dimensional electron-hole gases. *Phys. Rev. B* **79,** 045320 (2009).
59. You, Y. *et al.* Observation of biexcitons in monolayer WSe$_2$. *Nat. Phys.* **11,** 477–481 (2015).

Acknowledgements

Author contributions

S.C. and H.C. conceived the idea and designed the experiments. H.H., J.H.S. and M.-H.J. fabricated and characterized vapour-phase-grown MoS$_2$ monolayer crystals; and S.C., S.S. and J.P. conducted the ultrafast optical pump–probe spectroscopy. S.C., J.H.S. and S.S. analysed the results. All authors discussed the results and prepared the manuscript.

Additional information

Supplementary Information accompanies this paper at http://www.nature.com/naturecommunications

Competing financial interests: The authors declare no competing financial interests.

Reprints and permission information is available online at http://npg.nature.com/reprintsandpermissions/

How to cite this article: Cha, S. *et al.* 1*s* intraexcitonic dynamics in monolayer MoS$_2$ probed by ultrafast mid-infrared spectroscopy. *Nat. Commun.* 7:10768 doi: 10.1038/ncomms10768 (2016).